IOPscience iopscience.iop.org

Home Search Collections Journals About Contact us My IOPscience

Electronic and structural phase separation in strongly correlated sytems

This article has been downloaded from IOPscience. Please scroll down to see the full text article.

2003 J. Phys. A: Math. Gen. 36 9165

(http://iopscience.iop.org/0305-4470/36/35/305)

View the table of contents for this issue, or go to the journal homepage for more

Download details:
IP Address: 171.66.16.86
The article was downloaded on 02/06/2010 at 16:31

Please note that terms and conditions apply.

INSTITUTE OF PHYSICS PUBLISHING JOURNAL OF PHYSICS A: MATHEMATICAL AND GENERAL

J. Phys. A: Math. Gen. **36** (2003) 9165–9185 PII: S0305-4470(03)59994-2

Electronic and structural phase separation in strongly correlated sytems

J Lorenzana, C Di Castro and C Castellani

Center for Statistical Mechanics and Complexity, INFM, Dipartimento di Fisica, Università di Roma La Sapienza, P Aldo Moro 2, 00185 Roma, Italy

Received 21 February 2003
Published 20 August 2003
Online at stacks.iop.org/JPhysA/36/9165

Abstract

We review recent work on frustrated electronic phase separation in strongly correlated systems and the connection between electronic phase separation at a mesoscopic scale and structural phase separation at larger scales associated with volume instabilities. The former is due to the competition between phase separation tendencies and the long-range Coulomb interaction and surface energy effects. Above a critical value of the Coulomb interaction electronic phase separation is not possible and a volume instability arises. The system shows the tendency to phase separate into two neutral phases with different unit cell volumes.

PACS numbers: 64.75.+g, 71.10.Hf, 71.10.Ca

1. Introduction

Doped correlated insulators show a natural tendency to phase separate (PS) into carrier (electron or hole) rich regions and carrier poor regions for doping close to the insulating phase [1–4]. This inhomogeneity of charge is frustrated by the long-range Coulomb interaction.

The giant magnetoresistant manganites are a prominent example of these phenomena. Nagaev and collaborators predicted in the 1970s the appearance of drops of metal hosted by the insulator or vice versa for a doping range close to the parent compound [1]. Drops have been observed in $La_{1-x}Ca_xMnO_3$ [5] in good agreement with Nagaev's prediction.

On modelling homogeneous strongly correlated systems the long-range Coulomb (LRC) interaction is often neglected. This is because at long distances, exchange and correlation effects are irrelevant and hence the effect of the long-range interaction is to renormalize the Madelung potential by an irrelevant constant. In doing so one is implicitly treating Coulomb interactions in the Hartree approximation. Short-range interactions cannot be neglected since they have important dynamical effects giving rise to all variants of Hubbard-like models.

Clearly this framework breaks down when one considers non-uniform phases. The simplest generalization for non-homogeneous phases of the usual short-range models used

 © 2003 IOP Publishing Ltd Printed in the UK

in condensed matter theory is to treat the long-range interaction at the Hartree level. This takes correctly into account the 'tails' of the long-range Coulomb interaction that are usually neglected while keeping the short-range simplicity of the models [6–8]. As a first step one solves the short-range model for uniform phases and then considers nonuniform mixed phases and at the same time adds the long-range effects as an electrostatic correction to the energy. One has also to include an interface energy cost.

For simplicity we assume that the size of the inhomogeneities is mesoscopic, i.e. much larger than the interparticle distance. As in the ordinary Maxwell construction our results are independent of the specific nature of the two phases. This is in contrast with the more complicated case in which the scale of the inhomogeneities is of the order of the interparticle distance and the resulting texture is determined by the details of both short- and long-range interactions on an equal footing [3].

In our case because of the mesoscopic hypothesis the inhomogeneities can be treated as charged classical objects which order in a regular array. At each density the distance between inhomogeneities and their size is determined by the competition between the long-range Coulomb interaction and the interface boundary energy. Both effects introduce an energy cost (hereafter the mixing energy) and tend to frustrate the phase-separated state.

Assuming a uniform density (uniform density approximation (UDA)) within each phase we obtain the coexistence equations which generalize the Maxwell construction to the present situation. These equations can be applied to different geometries of the inhomogeneities (drops, layers, etc). Their solution is presented when each phase can be simply characterized in terms of a few density independent physical parameters (e.g. compressibility, etc). The physics is controlled by a dimensionless coupling constant λ which is given by the ratio of the characteristic energy loss due to the mixing energy and the characteristic energy gain due to the tendency towards PS obtained by the Maxwell construction. We find that: (i) the coexistence region shrinks as λ increases and the uniform phases are stabilized for densities at which a Maxwell construction in the absence of long-range Coulomb interaction would predict a PS state. (ii) The transition to the mixed state is abrupt in contrast with ordinary Maxwell construction. (iii) The densities of the local phases depend on the global density n, again in contrast with Maxwell construction, giving rise to novel nonlinear effects. (iv) The inhomogeneity radius is of the order of or smaller than the electric field screening length. (v) If the two phases are both compressible, a critical value of the coupling constant (λ_c) exists above which mesoscopic PS is not possible. In the latter case two situations can occur depending on the nature of the uniform phases. If the uniform phases can be connected continuously the system is always in a uniform neutral single phase. If the electronic free energies have instead a crossing point at a critical density n_c, a lattice instability occurs close to n_c leading to coexistence of two uniform neutral phases with different unit cell volumes. This 'structural' phase separation is similar to the volume collapse transition observed in mixed valence systems and we expect a similar phenomenology [9, 13].

2. Free energy and coexistence equations: the uniform density approximation

We consider a density-driven first-order phase transition in the presence of the LRC interaction and surface energy. We look for the formation of a mixed state by increasing the density from the uniform A phase. We use two different geometries for the mixed state. (i) The drop geometry consists of a Wigner crystal of drops of B phase in the host phase A. (ii) The layered geometry is made of a periodic array of alternating layers of A and B phases.

For both geometries the electronic density within each single-phase region is taken as uniform (UDA) and in general it will give a different result from the compensating background

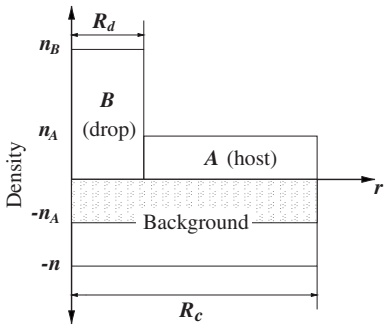

Figure 1. Schematic view of a cell density profile in the UDA with a drop (layer) of B phase in the host A. The origin is at the centre of the cell. The full cell diameter (width) is $2R_c$ for drops (layers). The dashed region of the background compensates the A density and part of the B density.

density. This is of course an approximation since both densities will tend to adjust within each phase also, to make the total electrochemical potential constant. The UDA will be relaxed in section 4 for the layered geometry by minimizing a free energy functional on a simple local density approximation (LDA). We anticipate here that both the UDA and the LDA give very similar results thus justifying our extensive use of the UDA.

We start by computing the total free energy. In the same spirit of the MC we assume that the free energies of hypothetically homogeneous bulk phases are known and given by F_A and F_B. We define the mixing energy E_m as the sum of the total surface energy and electrostatic energy (computed below). We work at a fixed total volume V and number of particles N. At a given temperature the total free energy is $F = F_B(V_B, N_B) + F_A(V_A, N_A) + E_m$. We have to minimize this with respect to V_B and N_B subject to the conditions $V_B + V_A = V$, $N_B + N_A = N$. The volume fraction of the B phase is $x \equiv V_B/V$. We can work with the free energies per unit volume $f \equiv F/V$, $e_m \equiv E_m/V$, $f_B \equiv F_B(V_B, N_B)/V_B$ and with the densities $n_B \equiv N_B/V_B$, etc so that the function to minimize is

$$f = (1-x)f_A(n_A) + xf_B(n_B) + e_m. \tag{1}$$

The constraint on the number of particles is written as $n = xn_B + (1-x)n_A$ and the constraint on the volume is satisfied by putting $V_B/V = 1 - x$. It is convenient to define $\delta \equiv n_B - n_A$ and to use the constraint in the number of particles to eliminate n_B and n_A in favour of n and δ.

In order to compute the mixing energy we first consider the drop geometry. We assume that the drops are spheres of radius R_d. This will be a good approximation as long as x is small and the crystal field is also approximately spherical. This is true for fcc, bcc and hcp lattices [10, 11]. To compute the electrostatic energy we use the Wigner–Seitz approximation [1, 10, 11]. We divide the system into slightly overlapping spherical cells each one with the volume $4\pi R_c^3/3 = V/N_d$ where N_d is the number of drops and R_c is the radius of the cell. Figure 1 shows a schematic view of the cell density profile.

Next we compute the electrostatic energy. The cells are globally neutral (by construction) and only the charge inside the cell contributes to the electric field in the cell.

The charge density of phase B is n_B (actually $-en_B$ but we drop the charge of the particles $-e$ for simplicity). The dashed background charge density in figure 1 ($-n_A$) compensates the A charge density n_A, and a slice of height n_A of the B charge density. For the purpose of computing the electrostatic energy these charge densities can be eliminated and one is left with the density $n_B - n_A(=\delta)$ inside the drop and $-(n - n_A)$ for the background. We will

call the former the 'drop contribution' and the latter the 'background contribution'. There is no 'host' contribution due to the above cancellation.

Another assumption is that the charge is spread uniformly and that microscopic discreetness effects can be neglected. One can see that corrections to the electrostatic energies due to discreetness are of order a^2/R_d^2 where a is the characteristic length of the microscopic structure (for example a lattice constant). Therefore they are negligible in our analysis which considers $R_d \gg a$.

With the above approximations the total electric field inside the cell is written as $\mathbf{E} = \mathbf{E}_b + \mathbf{E}_d$ where b (d) refers to the background (drop) contribution. Integrating the square of the electric field we obtain three contributions to the electrostatic energy: $\epsilon = \epsilon_d + \epsilon_b + \epsilon_{d-b}$ with

$$\epsilon_d = \frac{1}{8\pi\epsilon_0}\int \mathrm{d}^3 r\, \mathbf{E}_d^2 \tag{2}$$

with ϵ_0 the static dielectric constant and a similar equation for the background. The interaction energy is

$$\epsilon_{d-b} = \frac{1}{4\pi\epsilon_0}\int \mathrm{d}^3\mathbf{r}\, \mathbf{E}_b\mathbf{E}_d. \tag{3}$$

The use of the static dielectric constant is well justified because we are assuming a static super-structure which certainly will produce relaxation of the ions which in turn will screen the electric field. We are assuming by symmetry that the electric displacement is parallel to the electric field. The fields can be easily evaluated with Gauss theorem. One obtains

$$\epsilon_d = Q^2\frac{3}{5\epsilon_0 R_d} \tag{4}$$

$$\epsilon_b = Q^2\frac{3}{5\epsilon_0 R_c} \tag{5}$$

$$\epsilon_{d-b} = \frac{3Q^2}{\epsilon_0}\left(-\frac{1}{2R_c} + \frac{R_d^2}{10R_c^3}\right) \tag{6}$$

where $Q \equiv -e\delta v_d$ is the effective charge inside the drop. The volume of a drop is $v_d = 4\pi R_d^3/3$ and the number of drops is given by $N_d = V_B/v_d = xV/v_d$. We also have that $x = R_d^3/R_c^3$. Finally the total electrostatic energy per unit volume can be put as

$$e_e = \frac{2\pi e^2\delta^2}{5\epsilon_0}R_c^2 x^{5/3}(2 - 3x^{1/3} + x). \tag{7}$$

Setting one of the densities in δ to zero one recovers the expressions obtained by Nagaev and collaborators for the particular case of a mixed state composed of an antiferromagnetic insulating phase and a ferromagnetic metallic phase [1, 12].

The surface energy is parametrized by a quantity σ with dimensions of energy per unit surface. In general σ will be a function of the densities n_A, n_B. The total surface energy per unit volume is

$$e_\sigma = 4\pi\sigma R_d^2\frac{N_d}{V} = \frac{3\sigma x^{2/3}}{R_c}. \tag{8}$$

These two contributions add to give the mixing energy per unit volume $e_m = e_e + e_\sigma$.

Due to the constraint we have three parameters to determine (δ, x, R_c). The mixing energy is the only contribution which depends explicitly on the geometry. We can therefore eliminate R_c in favour of δ and x by minimizing e_m with respect to the cell radius to get

$$R_c = \left(\frac{15\sigma\epsilon_0}{4\pi x(2 - 3x^{1/3} + x)e^2\delta^2}\right)^{1/3}. \tag{9}$$

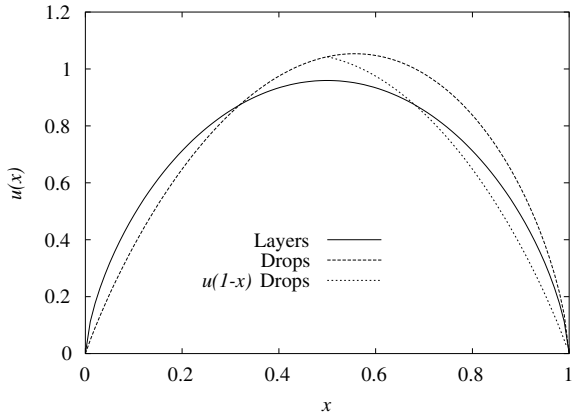

Figure 2. The function $u(x)$ that parametrizes the mixing energy for the layer geometry and the drop geometry.

Now we consider the layered geometry. The cell consists of a layer of width $2R_c$. The centre of the cell is occupied by a layer of width $2R_d$ of B phase and the rest is occupied by A phase. Figure 1 serves as a schematic plot of the density profile also in this case. r is a coordinate perpendicular to the layers with the origin at the centre of the B layer. The volume fraction now is given by $x = R_d/R_c$. By following analogous arguments as for the drops we obtain

$$e_e = \frac{2\pi e^2}{3\epsilon_0}\delta^2 R_c^2 x^2(1-x)^2 \tag{10}$$

$$e_\sigma = \frac{\sigma}{R_c} \tag{11}$$

$$R_c = \left(\frac{3\sigma\epsilon_0}{4\pi x^2(1-x)^2 e^2\delta^2}\right)^{1/3}. \tag{12}$$

Once R_c has been eliminated for both geometries the mixing energy can be put as

$$e_m = \left[\frac{\sigma^2 e^2\delta^2}{\epsilon_0}\right]^{1/3} u(x) \tag{13}$$

where all the geometric information is stored in $u(x)$:

$$u(x) = 3^{5/3}\left(\frac{\pi}{10}\right)^{1/3} x(2-3x^{1/3}+x)^{1/3} \quad \text{(drops)} \tag{14}$$

$$u(x) = \left(\frac{\pi}{2}\right)^{1/3}[3x(1-x)]^{2/3} \qquad \text{(layers)}. \tag{15}$$

In figure 2 we plot $u(x)$.

The free energy should remain invariant with respect to an exchange $A \leftrightarrow B$ and $x \leftrightarrow 1-x$. We will term this as 'phase exchange symmetry'. Figure 2 shows that this symmetry is only approximately realized by the $u(x)$ for drops. The deviation is due to the fact that the surface energy is minimized when the minority phase inhomogeneities are spherical. Our drop solution imposes this at small x but violates this in the opposite case of $x \to 1$, where the minority phase inhomogeneities have a complicated geometry defined by the interstitial region between the spherical drops.

A better treatment should allow for a switch from the unoptimized interstitial geometry to a spherical geometry at $x > 1/2$ with an energy gain given by the exchange of $u(x)$ in $u(1-x)$ as shown in figure 2. A comparison between the reflected curve and the original $u(x)$ shows that this geometry optimization compared to an apparently very bad geometry gives rise to a modest lowering of the energy. The same happens when we switch from the layered geometry to the spherical drop geometry as shown in figure 2. We can conclude that the dependence on geometry is weak.

The spherical drop geometry has lower energy than the layered geometry as expected from general arguments on surface tension but close to $x = 1/2$. Here our spherical drop solution is not adequate in any case. In fact in this region drops and the crystal potential will be far from spherical.

To avoid the complications of switching from different geometries we define a symmetrized drop function given by

$$u(x) = 3^{\frac{5}{3}} \left(\frac{\pi}{5}\right)^{\frac{1}{3}} \left\{ x(1-x) - \frac{[x(1-x)]^{\frac{4}{3}}}{2} \right\} \qquad \text{(symm. drops)}$$

which interpolates smoothly between the correct drop geometry in the limits $x \to 0$ and $x \to 1$. To determine the optimal geometry at intermediate x is beyond the scope of this work; however, as apparent in figure 2, $u(x)$, and consequently all our results, are weakly sensitive to the particular geometry considered.

We can also define a symmetrized drop radius that interpolates smoothly between the B drop radius at small x and the A drop radius for x close to 1:

$$R_d = \left(\frac{15\sigma}{\pi e^2 \delta^2}\right)^{1/3} \frac{1}{2 - [x(1-x)]^{1/3}}. \tag{16}$$

This expression for R_d is strictly valid close to $x = 0, 1$, otherwise it has the meaning of a typical inhomogeneity size.

Although the layer solution has higher energy due to its simplicity it is an excellent test ground for checking the approximations. We take advantage of this fact to test the UDA approximation in section 4.1. In addition the layer geometry has the extra advantage that, by construction, it respects the phase exchange symmetry.

Anyway since $u(x)$ depends weakly on geometry our results for macroscopic thermodynamic quantities will be largely independent of the geometry itself. When possible we present our results in a geometry-independent way by leaving the function $u(x)$ unspecified in our expressions. Minimizing the free energy with respect to δ and x one obtains

$$\mu_B - \mu_A = -\frac{2(e\sigma)^{2/3} u(x)}{3(\epsilon_0 \delta)^{1/3} x(1-x)} + \frac{2(e\delta)^{2/3} u(x)}{3\epsilon_0^{1/3}\sigma} \left(\frac{1}{x} \frac{\partial \sigma}{\partial n_A} - \frac{1}{1-x} \frac{\partial \sigma}{\partial n_B} \right) \tag{17}$$

$$p_B - p_A = (\mu_B - \mu_A)[n + \delta(1-2x)] + \left(\frac{e^2\sigma^2\delta^2}{\epsilon_0}\right)^{1/3} u'(x) - \frac{2\delta^{5/3} e^{2/3} u(x)}{3(\epsilon_0\sigma)^{1/3}} \left(\frac{\partial \sigma}{\partial n_A} + \frac{\partial \sigma}{\partial n_B} \right). \tag{18}$$

Here $p_A = -f_A + \mu_A n_A$, ($\mu_A = \partial f_A / \partial n_A$), etc are the 'intrinsic' pressures (chemical potentials) of each phase. The word 'intrinsic' stands for the values of these quantities in the presence of a fictitious fully compensating background, in other words they refer to a uniform single-phase situation. Equations (17), (18) determine the jump in these quantities at the interface in order to have thermodynamic equilibrium when long-range Coulomb forces

and surface energy are present. These equations are valid for a general geometry described by the function $u(x)$. Note that as long as $u(x)$ preserves the phase exchange symmetry the equations also preserve this symmetry.

To analyse the effect of the long-range forces and of the surface energy in the jumps let us neglect for simplicity the density dependence of the surface energy ($\partial\sigma/\partial n_A = \partial\sigma/\partial n_B = 0$) and concentrate on the drop geometry. Due to the different charge distributions, the electrostatic potential energy $-e\phi$ of an electron inside and outside the drops is different. In equilibrium this jump in the electrostatic potential should be compensated by a jump of the intrinsic chemical potentials (equation (17)) to make the electrochemical potential constant in the whole system. For $\delta > 0$ the drop repels electrons so the electrostatic potential energy will be lower outside the drop, i.e. $-e\phi_A < -e\phi_B$. The intrinsic chemical potential outside will have to be larger than inside as the sign in equation (17) implies.

Regarding the pressure, in equilibrium the intrinsic pressure inside the drop, p_B, should equal the pressure exerted by the host p_A plus the pressure exerted by the mixing forces. For $\delta > 0$ the electrostatic energy induces a negative contribution to the pressure since an increase in the drop volume at constant particle number decreases the difference in densities between the interior and the exterior of the drop and hence the Coulomb cost. This effect is given by the first term in equation (18). The second term proportional to $u'(x)$ is a geometric contribution.

In the limit $e \to 0$ one gets $\mu_B = \mu_A = \mu$ and $p_A = p_B = p$, i.e. $\mu\delta = f_B - f_A$, which are the conditions for MC.

3. General analysis of the mixed state in the uniform density approximation

In this section we set up the basic ideas for inhomogeneous solutions. For simplicity we model each phase free energy with a parabola and assume that the surface tension is density independent. Without loss of generality we write the parabolas as a quadratic expansion around the MC densities:

$$\begin{aligned} f_A(n_A) &= f_A^0 + \mu^0\left(n_A - n_A^0\right) + \frac{1}{2k_A}\left(n_A - n_A^0\right)^2 \\ f_B(n_B) &= f_B^0 + \mu^0\left(n_B - n_B^0\right) + \frac{1}{2k_B}\left(n_B - n_B^0\right)^2. \end{aligned} \tag{19}$$

The quantities with the '0' superscript (or subscript below) satisfy MC in the absence of LRC forces, i.e. $f_B^0 - f_A^0 = \mu^0\delta_0$ and $\delta_0 = n_B^0 - n_A^0$. The linear slope μ^0 is the same for the two phases due to the MC condition. The MC density n_0 and the volume fraction are related by $n_0 = n_A^0 + \delta_0 x$. The constants k_A, k_B are essentially the compressibilities of the two phases.

For non-interacting electrons at $T = 0$ the compressibility coincides with the density of states. For the 3D free electron gas we have

$$k_{\text{free}} = \frac{3^{1/3} m n_0^{1/3}}{\pi^{4/3}\hbar^2} \tag{20}$$

with m the electronic mass.

For a band of spinless electrons of width W and a flat density of states per unit volume given by $1/(a^3 W)$ the free energy at zero temperature is parabolic so the expansion of equation (19) is exact. The chemical potential is given by $\mu_0 = W a^3 n_0 + \Delta_0$ with Δ_0 a band-dependent shift related to the Madelung potential and the compressibility given by

$$k_{\text{flat}} = \frac{1}{W a^3}. \tag{21}$$

Another useful realization is a nondegenerate gas where we have

$$k_{\rm gas} = \frac{n_0}{KT}. \tag{22}$$

Our aim in the following is to obtain the equations which control the deviation from MC behaviour in the presence of the mixing energy.

We define a dimensionless global density

$$n' \equiv \left(n - n_A^0\right) \Big/ \delta_0$$

which measures the distance from the point in which the B phase appears in the absence of Coulomb forces. In MC the coexistence region is given by $0 < n' < 1$.

Equations (17), (18) determine δ, and x for a fixed density where now μ_A, μ_B, p_A and p_B can be expressed in terms of the parameters appearing in equations (19).

In practice it is much easier to solve the equations by fixing the volume fraction x and solving for δ and n, i.e. we find which density one should put in the system to obtain a mixed state with a given volume fraction. This is because the solutions happen to be multivalued functions of n whereas they are single-valued functions of x (see below).

For a fixed volume fraction x we define the dimensionless density deviations from the MC values: $\hat{n} = (n - n_0)/\delta_0$ and $\hat{\delta} = (\delta - \delta_0)/\delta_0$. The density deviation $\hat{n}$ measures the shift in the global density needed to have the same volume fraction of a system without LRC interaction.

To fix the energy units it is convenient to choose one of the two compressibilities as a reference, for example the largest. We define $k_m = \max(k_A, k_B)$. Energies per unit volume will be measured in units of the characteristic PS energy δ_0^2/k_m. The latter is essentially the difference between the uniform parabolic free energy and the MC free energy at the characteristic density δ_0.

Now we define two important reference length scales in the theory. The characteristic size of an inhomogeneity for which the Coulomb energy balances the surface energy is given by the R_c of the previous section with the geometric factors dropped and the density evaluated at the MC value. This defines the scale

$$l_d = \left(\frac{\sigma\epsilon_0}{e^2\delta_0^2}\right)^{1/3}. \tag{23}$$

The other length is given by $l_s^2 = \epsilon_0/(4\pi e^2 k_m)$. By relaxing the UDA we will show in section 4 that l_s is a screening length. In other words if the reference phase (the one with k_m) is interpreted as a metal, l_s is the characteristic distance which the electric field penetrates.

The theory has two dimensionless parameters. One is the ratio k_B/k_A. The other measures the strength of the mixing energy effects in units of the characteristic PS energy δ_0^2/k_m and is given by

$$\lambda = 2\frac{k_m}{\delta_0^2}\left(\frac{9\pi e^2\delta_0^2\sigma^2}{5\epsilon_0}\right)^{1/3} = \frac{1}{2}\left(\frac{9}{5\pi^2}\right)^{1/3}\left(\frac{l_d}{l_s}\right)^2. \tag{24}$$

The characteristic mixing energy is given by the factor with the power $1/3$ in the middle expression. The constant λ characterizes the competition of the mixing energy cost and the MC like energy gain due to phase separation. The coupling constant goes to zero as $e \to 0$ with σ finite. This corresponds to the usual PS. The case $\sigma \to 0$ with finite e corresponds to an infinite number of drops (or layers) of zero radius. In this maximum intermixing situation the charges of the two phases spatially coincide and the Coulomb cost also goes to zero so that the MC is again valid. Note however that this last idealized situation cannot be reached in practice because at some point for small drop radius the continuous approximation will fail.

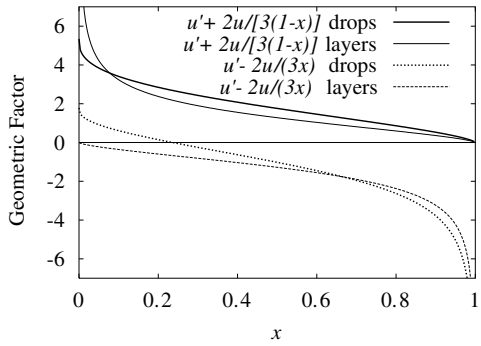

Figure 3. The dimensionless functions that determine the change in n_A (upper curves) and n_B (lower curves) for small λ versus the volume fraction x for the layered and the drop geometry (see equation (26)).

Inserting the explicit expressions (19) of f_A and f_B in equations (17), (18) we obtain the following equations for the density deviations:

$$\begin{aligned}
&\hat{n}\left(\frac{1}{k_B}-\frac{1}{k_A}\right)+\hat{\delta}\left(\frac{1-x}{k_B}+\frac{x}{k_A}\right)=\left(\frac{5}{9\pi}\right)^{1/3}\frac{\lambda u(x)}{3k_m(1+\hat{\delta})^{1/3}x(1-x)}\\
&\frac{x\hat{\delta}-\hat{n}}{k_A}+\left[\hat{n}\hat{\delta}(1-x)+\frac{\hat{n}^2}{2}\right]\left(\frac{1}{k_B}-\frac{1}{k_A}\right)+\frac{\hat{\delta}^2}{2}\left[\frac{1-2x}{k_B}+\frac{2x}{k_A}+\left(\frac{1}{k_B}-\frac{1}{k_A}\right)x^2\right] \qquad (25)\\
&\qquad=\left(\frac{5}{9\pi}\right)^{1/3}\frac{\lambda(1+\hat{\delta})^{2/3}}{2k_m}\left[u'(x)+\frac{2u(x)}{3(1-x)}\right].
\end{aligned}$$

The coexistence equations (25) can be solved numerically for general values of the parameters.

For small λ, i.e. for small mixing energy, we can linearize the equations neglecting higher order terms in $\hat{\delta}$ and $\hat{n}$. We will refer to this as the linearized UDA. The linearized solution takes a simple form and is explicitly symmetric with respect to an exchange of phases when written in the original variables:

$$\begin{aligned}
n_A&=n_A^0+\frac{1}{6}\left(\frac{15}{\pi}\right)^{1/3}\frac{k_A}{k_m}\lambda\delta_0\left[u'(x)+\frac{2u(x)}{3(1-x)}\right]\\
n_B&=n_B^0+\frac{1}{6}\left(\frac{15}{\pi}\right)^{1/3}\frac{k_B}{k_m}\lambda\delta_0\left[u'(x)-\frac{2u(x)}{3x}\right].
\end{aligned} \qquad (26)$$

In the case of $\lambda=0$, according to MC, the system separates into two phases with densities n_A^0, n_B^0 respectively independently of the volume fraction. For nonzero λ and small x the B phase divides into drops or layers and the density in each phase depends on the volume fraction of the B phase. The deviation of each density from the MC prediction is proportional to λ and to the compressibility of each phase. Note that the density of an incompressible phase ($k\to 0$) does not depend on the volume fraction even in the presence of LRC forces.

In figure 3 we show the behaviour of the two functions which determine the dependence of the densities on the volume fraction. In the drop geometry and for small x both n_A and n_B tend to be larger than in the MC case whereas in the layered geometry only n_A is larger. This gives rise to minor qualitative differences in the behaviour of drops and layers. Apart from this the overall behaviour is similar.

The equation for the density of one phase (equation (26)) has a transparent interpretation in the limit in which the other phase, say A, is incompressible ($k_A = 0$). Assume that the A phase is the vacuum and so exerts no pressure and has zero density. We can consider that the mixing forces due to the electrostatic and surface energies exert an 'external' pressure on the B phase inhomogeneity. In equilibrium the intrinsic pressure of the B phase (p_B) should compensate this 'mixing pressure' ($p_B = p_m$). The latter is given by

$$p_m = \frac{\partial e_m}{\partial x} - \frac{2e_m}{3x}. \tag{27}$$

On the other hand, a change in the external pressure corresponds to a change in the n_B density according to the B phase equation of state. This follows directly from our definition of compressibility:

$$k_B \equiv n_B^0 \frac{\Delta n_B}{\Delta p_B}$$

where we have replaced a derivative by a finite different ratio. We can obtain the second linearized expression in equation (26) directly from this definition using that the MC density corresponds to zero intrinsic pressure,

$$n_B - n_B^0 = k_B \frac{p_B}{n_B^0} \propto k_B n_B^0 \left[u'(x) - \frac{2u(x)}{3x} \right].$$

The mixing pressure can be negative. This implies that the density is less than the MC density. From the lower curves in figure 3 we see that for drops the pressure is positive for small x and then becomes negative whereas for layers the pressure is negative for all x.

Remarkably, in both cases the mixing pressure is a decreasing function of x. Since in general x is an increasing function of n' we can anticipate that n_B will decrease as n' increase (see below). This important effect has been used to explain the anomalous Curie temperature of manganites [7].

Note that for small x we have $p_B \sim u'(x)/3$ so a decreasing mixing pressure can be directly related to the negative curvature of $u(x)$ (figure 2).

Specific results will be presented in the next section for the drop geometry and in section 4.1 for the layered geometry.

3.1. Results of the UDA for the drop geometry

Now we switch to the symmetrized drop solution which we have obtained solving the coexistence equations numerically.

In figure 4 we plot the volume fraction as a function of global density for the drop solution. The volume fraction is a multivalued function of n' and in the case $k_B = k_A$ has a lower branch close to $x = 0$, an intermediate branch, and an upper branch close to $x = 1$. The intermediate branch is the physical solution. This will be shown below by looking at the free energy. The physical solution has the intuitive property that the volume fraction increases as global density increases.

We see that the bifurcation density $n'_{\rm bif}$ at which the phase-separated solution appears for finite λ is larger than in MC. On the other hand, the B phase appears with a finite volume fraction and its rate of growth is larger than in the MC case.

To decide the stability of the solution we have to compare the drop solution with the single-phase solution. In figure 5 we show $f_A(n')$, $f_B(n')$ and the total free energy with $k_B = k_A$ for various λ. The MC line $f^0(n') = f_A^0 + n'\left(f_B^0 - f_A^0\right)$ has been subtracted. The energy also is a multivalued function of n'. As the density increases the drop solution appears

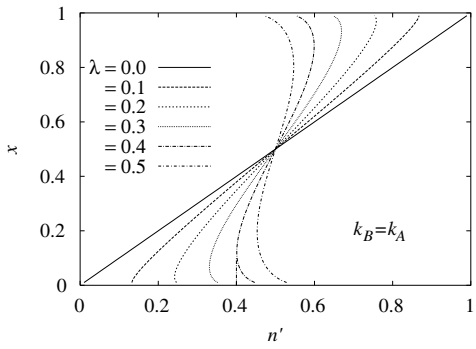

Figure 4. Volume fraction versus n' for (from left to right at the bottom) $\lambda = 0, 0.1$, 0.2, 0.3, 0.4, 0.5 and $k_B = k_A$ for symmetrized drops. For $\lambda = 0.4$ we indicate with a vertical line the discontinuity in the volume fraction to go from the uniform solution to the drop solution by increasing the density.

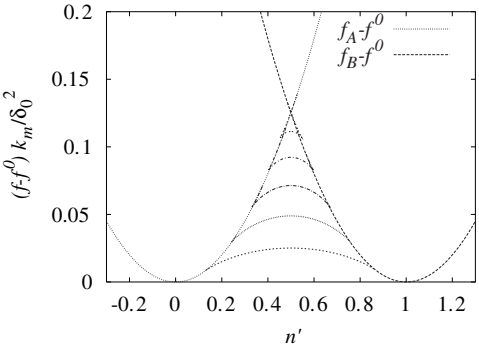

Figure 5. $f_A - f^0$, $f_B - f^0$ and $f - f^0$ in the symmetrized drop solution for $\lambda = 0.1$, 0.2, 0.3, 0.4, 0.5 (from bottom to top) and $k_B = k_A$ versus n'. Here f^0 is the MC free energy for $\lambda = 0$ (a straight line).

at $n'_{\rm bif}$ with two different branches. The upper branch overlaps with the uniform solutions. In the upper (unstable) branch x decreases with density. For the lower branch one finds the expected behaviour, i.e. x increases with density. Near the bifurcation the three solutions (homogeneous, drop stable and drop unstable) are very close in energy. We find that the bifurcation density $n_{\rm bif}$ is lower than the density n_c at which the energy of the lower energy drop solution crosses the energy of the uniform phase $f_A(n')$. The difference between n_c and $n_{\rm bif}$ is negligible for all practical proposes in the case $k_A = k_B$ as shown in the inset of figure 6.

When the phases are both compressible, a critical value of the coupling exists such that for $\lambda > \lambda_c$ the inhomogeneous state is not possible (figure 6). The uniform A–B boundary line is determined by the crossings of the parabolas in figure 5. The existence of a finite λ_c does not depend on the specific parametrization of equation (19). It rather depends on the existence of a maximum available PS energy gain per unit volume. More specifically, this gain is given by the largest difference between the Maxwell construction free energy and the most stable uniform free energy at each global density. If frustration increases at some point the mixing energy cost is not compensated by this energy gain.

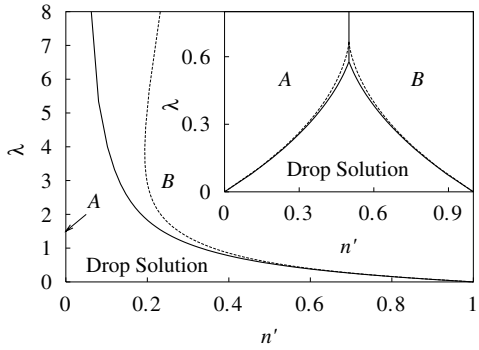

Figure 6. Phase diagram for $k_A = 0$ (full lines). The uniform A phase reduces to a line at $n' = 0$. The dotted line is $n'_{\rm bif}$, the limit of existence of the drop solution. Inset: the same for $k_A = k_B$.

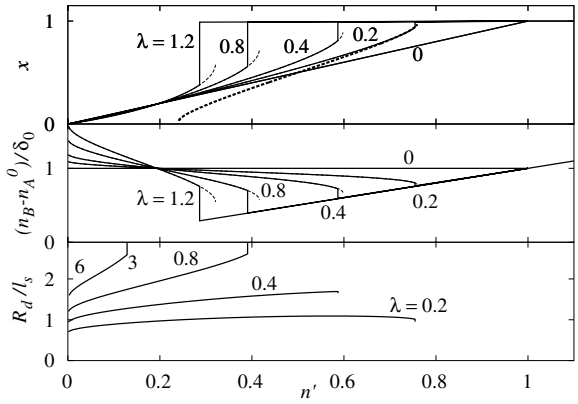

Figure 7. Volume fraction (top), local density of the B phase (middle) and symmetrized drop radius (bottom) as a function of global density for $k_A = 0$ and different λ. The vertical lines indicate the points where the drop solution becomes less stable than the uniform solution. The full lines are the lowest energy solutions whereas the thin dashed lines are the metastable solutions. The thick dashed line (top) is the volume fraction for $k_A = k_B$ and $\lambda = 0.2$.

When one of the compressibilities goes to zero, say k_A, the crossing moves to the left in figure 5 and the uniform A region shrinks until the boundary line for the uniform A phase approaches the MC value $\left(n = n_A^0\right)$. At the same time λ_c increases. This last case ($k_A = 0$) is representative of the coexistence of an insulator (A) with a metal (B).

In figure 6 we show the phase diagram in the λ–n' plane for the two limiting cases $k_A = k_B$ and $k_A = 0$. In both cases $k_A = k_B$ and $k_A = 0$ one sees that as λ increases the n' range of stability of PS shrinks (point (i), section 1). When the host phase is incompressible, one sees from figure 6 at small n' that a drop state is stable no matter how big λ is. Indeed, in this case the PS energy gain stays finite at n_A^0 (the Maxwell construction density), whereas the energy cost $e_m \sim u(x) \sim x \sim n'$ vanishes.

In figure 7 we report the behaviour of the symmetrized drop radius, volume fraction and the density of the B phase as a function of the global density for $k_A = 0$.

The behaviour of the system close to the threshold for the appearance of drops is largely independent of the compressibility of the drops and is mainly determined by that of the host. Indeed, the boundary line (figure 6) is very similar for $k_A = 0$ and for $k_A = k_B$ when $n' > 1/2$

where B plays the role of the host. To further illustrate this point we also show in figure 7 the volume fraction for $k_A = k_B$ and $\lambda = 0.2$ (thick dashed line). Near the threshold density ($n' \approx 0.76$) (for both $k_A = 0$ and $k_A = k_B$) the curves practically coincide. Therefore, the case $k_A = 0$ alone contains the two physically relevant cases of an incompressible host (A) for small n' and a compressible host (B) for large n'. Because of this we analyse this case in more detail.

Starting from $n' = 1$ and reducing n' at fixed λ one switches from the uniform B phase ($x = 1, n_B = n$) to the A drop state (figure 7). For the generic case of a compressible host the transition is abrupt with a discontinuity of both the volume fraction and the local density (point (ii), section 1). Reducing the density further the two phases exchange their role and the host is the incompressible phase A. In this case (incompressible host) the transition is continuous as can be seen from the fact that x goes continuously to zero when $n' \to 0$. Indeed the mixing energy, responsible for the nonlinearities, becomes irrelevant in this limit as explained above.

Remarkably, in contrast to the Maxwell construction, the local density n_B depends on the global density (figure 7) and more interestingly it increases as the global density decreases (point (iii), section 1). This behaviour is generic for compressible phases, independent of the ratio k_A/k_B and can give rise to unexpected effects in real systems. Any physical quantity that depends on the local density will have an anomalous behaviour in the coexistence region. We have recently proposed that this may be the reason why some manganites have regions of doping where the doping dependence of the Curie temperature ($\mathrm{d}T_c/\mathrm{d}n$) has opposite sign with respect to the double exchange predictions. We assume a FPS state where the T_c of ferromagnetic inhomogeneities depends on the local density rather than the global one [7].

Independently of k_A/k_B the drop radius R_d behaves as $2\sqrt{\lambda}l_s$ for small λ and saturates to a value close to $2l_s$ for large λ with some smooth variation around these values upon varying the global density (figure 7). Generically inhomogeneities can only appear if they are small enough that the electric field can penetrate them (point (iv), section 1). Indeed for large λ and $k_A = 0$ only soft phase (B) drops are allowed (n' small, figure 6) and the radius $R_d \sim 2l_s$ is of the order of the screening length in the drops. For small λ since l_s is the smallest screening length among A and B and $R_d \sim 2\sqrt{\lambda}l_s \ll l_s$, drops are penetrated by the field independently of k_A/k_B. We mention that the same criterion applies to the interstitial regions.

This behaviour is better understood when the UDA is relaxed (section 4).

Another peculiarity of the curves in figure 5 is that the free energy of the drop solution has the 'wrong' curvature, that is the compressibility (defined from $\partial^2 f/\partial^2 n$) is negative. This does not necessarily imply an instability since the usual stability condition of positive compressibility is formulated for a neutral system, that is including the background compressibility. Since we are assuming the inverse background compressibility to be an infinite positive number (in our analysis the background density has a fixed homogeneous value) it follows that the total compressibility is positive and from this point of view the system is in a stable mixed state. Of course, this does not guarantee stability against more complicated solutions than the simple crystal of drops. The situation is more severe for $\lambda > \lambda_c$ (see below).

Two situations can then occur. The two phases in the absence of long-range Coulomb interaction can be connected continuously through the instability region as in van der Waals treatment of the liquid gas transition. In this case one expects that the first derivative of the bulk free energy with respect to the density is continuous and the second derivative (the compressibility) is negative in some range. For $\lambda > \lambda_c$ this finite negative compressibility is compensated by the background which we assume to have a very large positive inverse compressibility and the whole system is in a stable single phase at all densities.

When instead the two phases cannot be connected continuously, e.g. because of a symmetry mismatch, the bulk free energies should cross at a critical density n_c just as in our simple parametrization of equation (19). For $\lambda > \lambda_c$ the transition occurs at n_c between the two uniform phases. Then a severe problem occurs because the free energy has a cusp pointing up at n_c and the electronic inverse compressibility is minus infinity. The system cannot be stabilized by the large but finite positive inverse compressibility of the background. Clearly in this situation one has to consider that the background is compressible from the beginning. We have therefore extended the expansion of equation (19) and allowed the background volume per formula unit to be different in the two phases with a certain lattice compressibility. The free energy as a function of the unit cell volume consists now of a parabola with positive curvature given by the lattice compressibility plus a pointing up cusp due to the singular electronic contribution. As a result one has a two-minima structure for the total free energy. In this case a standard Maxwell construction analysis gives a coexistence between neutral phases with different unit cell volumes (point (v), section 1). The problem of nucleation in this case is very anomalous as in mixed valence systems [13].

The same argument applies at the critical density where the drop solution crosses the uniform solution, although the negative dip is much less pronounced in that case (see figure 6). Usually the electronic system is a crystal where the background is provided by the ionic lattice. If one trys to prepare the crystal with an electronic density close to the critical one the system can break into two pieces, each one with a different lattice constant. Typically the crystal is not at a fixed volume but at a fixed external pressure P. (We use capital P to distinguish the pressure exerted on the crystal as a whole from the electronic pressures of the phases p_A and p_B.) In this situation MC determines the equilibrium pressure P_0 for phase coexistence. P_0 will depend on the global doping so, above λ_c, P_0 versus doping determines a phase boundary line which will cut ambient pressure at some critical doping. A large pressure hysteresis around the equilibrium pressure has recently been predicted [13]. This effect is well known to occur in mixed valence systems [9].

Since the electronic free energies depend on external parameters, a remarkable implication is that the critical doping will also depend on external parameters such as magnetic field, temperature, pressure, etc. In other words a crystal can be driven from a single phase to a two-phase situation by changing external parameters. This explains the situation in some manganites where one finds that a single-phase crystal breaks in a multidomain crystal by lowering the temperature. The multidomain system shows lattice mismatch and large stress at the interfaces in agreement with our analysis. [14, 15]

In section 4.1 analogous results are presented for the layered geometry case and compared with a more elaborate computation which relaxes the UDA. In [7] we present more specific applications to different physical systems.

4. Local density approximation

In this section we generalize our results to take into account the full spatial dependence of the density. The basic assumption is that we can write the free energy of each phase as the spatial integral of a free energy density which is a function of the local density, i.e. we are using a local density approximation (LDA). The free energy reads

$$F = \int_{\mathbf{r}\in A} \mathrm{d}^3\mathbf{r}\, f_A[n(\mathbf{r})] + \int_{\mathbf{r}\in B} \mathrm{d}^3\mathbf{r}\, f_B[n(\mathbf{r})] + \frac{1}{8\pi}\int \mathrm{d}^3\mathbf{r}\, \mathbf{E}^2 + S_{AB}\sigma. \tag{28}$$

Here $\mathbf{r} \in A$ indicates that the integral is restricted to the regions of phase A and S_{AB} is the total interface surface between A and B and we assume for simplicity $\epsilon_0 = 1$. One should

be careful not to double count in σ surface energy costs that are due to the spatial variation of the charge since this will be explicitly taken into account in the first three terms. On the other hand, one can include in σ other effects, such as magnetic, which would not be included otherwise. For simplicity we will assume σ to be density independent.

The electric field is related to the total charge density (electronic plus background) through the Poisson equation

$$\nabla \cdot \mathbf{E} = 4\pi\rho \tag{29}$$

with the total charge density

$$\rho = -e[n(\mathbf{r}) - \bar{n}]. \tag{30}$$

Here $\bar{n}$ is the global density of the previous section and the bar distinguishes it from the spatially varying density $n(\mathbf{r})$. Note that $e\bar{n}$ is the charge density of the background. The condition of neutrality is written as

$$\bar{n} = \frac{1}{V}\int_{\mathbf{r}\in A} \mathrm{d}^3\mathbf{r}\, n(\mathbf{r}) + \frac{1}{V}\int_{\mathbf{r}\in B} \mathrm{d}^3\mathbf{r}\, n(\mathbf{r}). \tag{31}$$

Using $n(\mathbf{r}) = n_A$ for $\mathbf{r} \in A$ and $n(\mathbf{r}) = n_B$ for $\mathbf{r} \in B$ one recovers the UDA.

Instead of minimizing the functional with respect to the density it is convenient to use equations (29), (30) to express the density as a function of the electric field, ($n = n(\nabla.\mathbf{E})$) and minimize the functional with respect to the electric field profile. We look for periodic solutions (layer, crystal, etc) and restrict the computation to one cell.

Minimizing the free energy (equation (28)) with respect to the electric field one obtains

$$\mathbf{E} = -\frac{1}{e}\nabla\frac{\partial f_X}{\partial n}[n(\nabla \cdot \mathbf{E})] \tag{32}$$

where $X = A$ or B when $\mathbf{r} \in A$ or $\mathbf{r} \in B$ respectively. This differential equation together with the boundary condition determines the field profile. The boundary condition at the cell boundary and at the internal boundary will be discussed in the example below. Once the electric field profile is known for a given geometry the density profile is given by Poisson equation. As a final step one should optimize the geometry.

Introducing the parabolic expressions (19) to parametrize the free energy densities in equation (32) one obtains

$$\mathbf{E} = l_X^2 \nabla\nabla \cdot \mathbf{E} \tag{33}$$

with $l_X^2 = (4\pi e^2 k_X)^{-1}$. Clearly l_X is the screening length as anticipated in section 3. If we use the compressibility of a free electron gas for k_X (equation (20)) and reintroduce the dielectric constant, l_X corresponds to the Thomas–Fermi screening length

$$l_X^2 = \left(\frac{\pi}{3}\right)^{1/3} \frac{\epsilon_0\hbar^2}{4e^2 m\left(n_X^0\right)^{1/3}}. \tag{34}$$

We reach Thomas–Fermi theory which is the simplest version of the LDA used for electronic structure computations. If we use the nondegenerate gas compressibility [equation (22)] l_X is the Debye–Hückel screening length.

4.1. Solution for the layered geometry

In the layered geometry the differential equation (33) reduces to a one-dimensional problem and can be readily solved. The geometry is identical to that in the UDA approximation (figure 1). The central B layer has width $2R_d$ and the cell has width $2R_c$. The r coordinate is perpendicular to the layers and $r = 0$ corresponds to the centre of the B layer. By symmetry

the field is zero at $r = 0$ and $r = R_c$. In this case the boundary condition $\mathbf{E}_\perp = 0$ for the electric field perpendicular to the surface at the cell boundary automatically warrants the neutrality condition (31) due to Gauss theorem.

Apart from the cell boundary the cell itself has an internal boundary that divides A and B phases that we call E_0 the electric field at the A–B boundary. The value of E_0 is also optimized and this provides an additional boundary condition.

The solution is of the form

$$\begin{aligned} E_A(r) &= E_0 \frac{\sinh[(r - R_c)/l_A]}{\sinh[(R_d - R_c)/l_A]} \\ E_B(r) &= E_0 \frac{\sinh(r/l_B)}{\sinh(R_d/l_B)} \end{aligned} \tag{35}$$

where $E_A(r) \equiv E(r)$ for $r \in A$, etc.

The charge density is given by

$$\begin{aligned} \rho_A &= \frac{E_0}{4\pi l_A} \frac{\cosh[(r - R_c)/l_A]}{\sinh[(R_d - R_c)/l_A]} \\ \rho_B &= \frac{E_0}{4\pi l_B} \frac{\cosh(r/l_B)}{\sinh(R_d/l_B)}. \end{aligned} \tag{36}$$

The electric field at the A–B boundary can be related to the jump in the density at the interface

$$E_0 = \frac{-4\pi e[n_B(R_d) - n_A(R_d)]}{[l_B \tanh(R_d/l_B)]^{-1} + \{l_A \tanh[(R_c - R_d)/l_A]\}^{-1}}. \tag{37}$$

It plays the same role as the parameter δ in section 2 so that we can find the optimum charge distribution between A and B by minimizing the free energy with respect to E_0.

After replacing equations (36), (37) in the expression for the free energy (equation (28)) and minimizing with respect to E_0 we find

$$E_0 = \frac{4\pi e \delta_0 \left[l_B^2(n' - 1) - l_A^2 n'\right]}{l_B / \tanh(x R_c/l_B) + l_A / \tanh[(1 - x)/l_B]} \tag{38}$$

where δ_0 and n' are defined as in section 3 and R_d has been eliminated in favour of the volume fraction with $R_d = x R_c$.

At this point the total free energy per unit volume $f \equiv F/V$ takes the form

$$\begin{aligned} f = f_A^0 + \delta_0 \mu_0 n' + \frac{\sigma}{R_c} + 2\pi e^2 \delta_0^2 \left[l_A^2 (n')^2 (1 - x) + l_B^2 x (1 - n')^2\right] \\ - \frac{2\pi \delta_0^2 e^2 \left[-l_B^2(1 - n') - l_A^2 n'\right]^2}{R_c \{l_B / \tanh(x R_c/l_B) + l_A / \tanh[(1 - x) R_c/l_A]\}}. \end{aligned} \tag{39}$$

The first two terms are the MC free energy, the third term is the surface energy and the last two terms are both contributions due to the shift from the MC densities and due to the electrostatic energy.

The last step is to minimize this free energy with respect to the volume fraction and R_c. This gives two equations which can be solved numerically for R_c and x. As in section 3 it is easier to fix x and solve for R_c and n'.

In the following we present results for the case $k_B = k_A$ and compare with the linearized UDA of section 3 for the layered geometry.

In figure 8 we plot the volume fraction as a function of global density in the LDA approximation and the UDA approximation. Clearly the results are very similar even quantitatively. In the UDA there is a jump in the volume fraction from zero to a finite

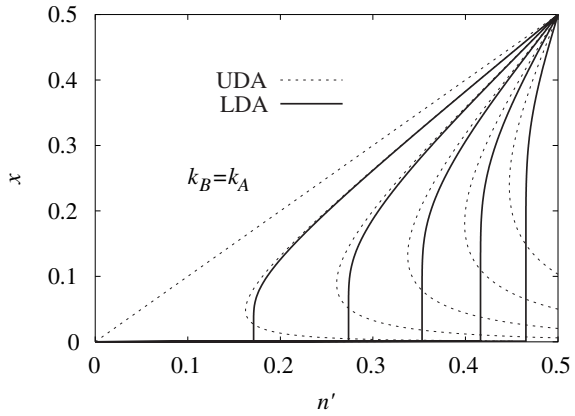

Figure 8. Volume fraction versus n' for (from left to right at the bottom) $\lambda = 0, 0.1, 0.2, 0.3, 0.4, 0.5$ and $k_B = k_A$ in the LDA (thick lines) and the UDA (thin lines). Only the lower left corner of the plot is shown since the upper right corner is symmetric by phase exchange. For the UDA approximation the lower branch is unphysical as in section 3.1.

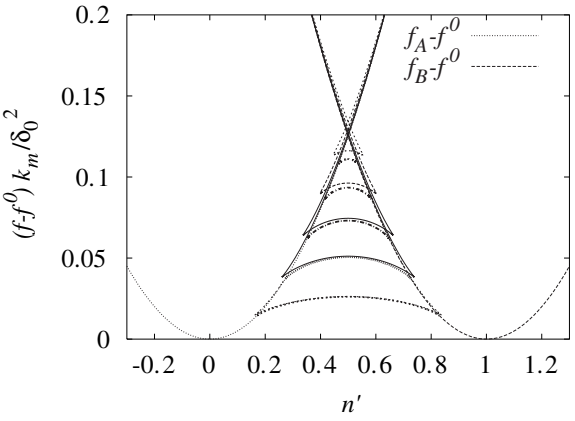

Figure 9. $f_A - f^0$, $f_B - f^0$ and $f - f^0$ in the layered solution for $\lambda = 0.1, 0.2, 0.3, 0.4, 0.5$ (from bottom to top) and $k_B = k_A$ versus n' in the LDA (thick lines) and the UDA (thin lines). Here f^0 is the MC free energy for $\lambda = 0$ (a straight line).

value. In the LDA the volume fraction is not discontinuous but grows very rapidly at the threshold for the appearance of the inhomogeneous state. Another important difference is that the solutions are no longer multivalued in the LDA.

In figure 9 we show $f_A(n')$, $f_B(n')$ and the total free energy with $k_B = k_A$ for various λ. The MC line $f^0(n') = f_A^0 + n'\left(f_B^0 - f_A^0\right)$ has been subtracted. The behaviour of the layered solution in the UDA is similar to that found for drops in section 3.1 and coincides with it at small λ. In the LDA approximation multivaluation disappears. The relaxation of the UDA approximation obviously produces a gain in energy since the functional that we are minimizing is the same in LDA and the UDA but in the UDA we are imposing an extra constraint on the densities. The gain in energy however is quite small. The phase diagrams in the UDA and LDA (not shown) are both very similar (even quantitatively) to the one for drops of section 3.1 except that they are fully symmetric. The critical λ above which the inhomogeneous solution is never stable is given for $k_B = k_A$ by $\lambda_c = (9/5)^{1/3}/2 \sim 0.61$ in the LDA and by $\lambda_c \sim 0.70$ in the UDA.

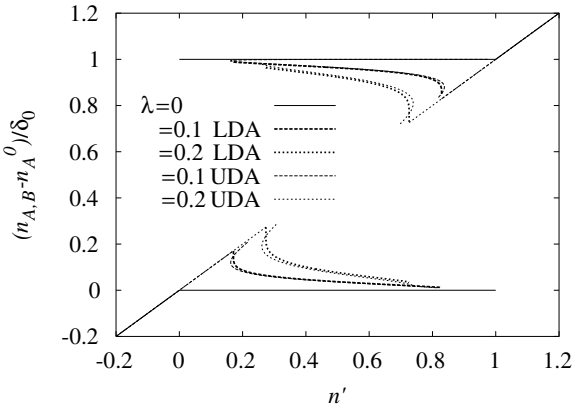

Figure 10. Normalized spatially averaged densities of each phase as a function of normalized global density n' for different λ, $k_B = k_A$ and the linearized UDA (thin lines) and the LDA (thick lines). The lower curves correspond to the A phase and the upper curves to the B phase. In the coexistence region multivalued densities appear in the linearized UDA. The long branch is the physical one.

In figure 10 we show the densities in each phase in the UDA. This is compared with the densities of each phase in the LDA averaged spatially over the space spanned by each phase. Again the behaviour is remarkably similar and the density discontinuities of the UDA become very steep changes with the LDA.

Finally in figure 11 we show the behaviour of the dimensions of the cell and of the B layer as a function of global density. Due to perfect phase exchange symmetry the cell width $2R_c$ as a function of n' is symmetric and has the minimum exactly at $n' = 0.5$. The discontinuous jump at the threshold in the UDA becomes a divergence in the LDA. For the same parameters the cell widths are smaller in the UDA than in the LDA. This can be understood by noting that in the UDA the widths are of order $l_s = [\sigma/(\delta_0 e)^2]^{1/3}$. Roughly speaking, we can say that the effect of the LDA is: (i) to increase the surface energy due to the bending of the charge distributions at the surface and (ii) to screen the electric fields which can be schematized as an effective reduction of the charge e. Both effects tend to increase the width of the layers as found.

For small λ figure 11 shows that the LDA and UDA radii coincide just as the full solution. This is because $l_d \sim \sqrt{\lambda} l_s \ll l_s$ (cf equations (23), (24)] so that the density is almost constant inside the layer even in the LDA and the solutions are virtually the same. In this case the Thomas–Fermi approximation is ineffective to generate a surface energy since all surface energy effects other than the ones explicitly included in σ are due to density variations. In other words, if one sets $\sigma = 0$ the system prefers to make small drops to avoid both the Thomas–Fermi-induced surface energy effect and the Coulomb cost. This however is a drawback of the Thomas–Fermi approximation since small drops will certainly have a large surface energy due to the confinement of the electron gas. It is well known that Thomas–Fermi theory is a poor approximation to model surfaces.

If one increases λ inhomogeneities are possible until the point at which $l_d \sim l_s$ and $\lambda = \lambda_c$. It is not possible to have inhomogeneities of dimension $l_d \gg l_s$ because in the region far from the surface screening makes the local density coincide with the global density and this inhibits any PS energy gain. It is then convenient for the system to avoid any surface and remain single phase.

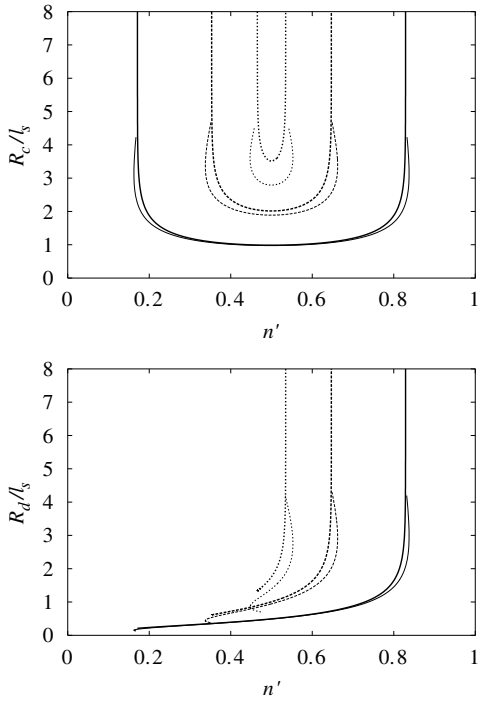

Figure 11. R_c and R_d in units of the screening length l_s defined above (equation (24)) versus n' in the linearized UDA (thin lines) and the LDA (thick lines). We show the curves for $\lambda = 0.1, 0.3, 0.5$ which increase from bottom to top in the top panel and from right to left at the top in the lower panel.

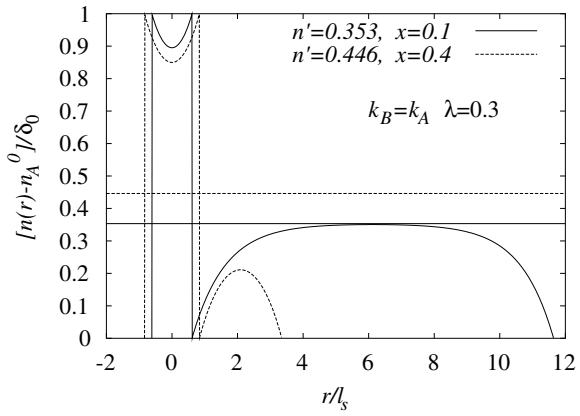

Figure 12. Density profile for $\lambda = 0.3$ and different values of the global density. The region close to $r = 0$ corresponds to the B phase and the rest is the A phase. The structure repeats periodically in the r direction. The horizontal lines signal the global density.

In figure 12 we show the density profile for $\lambda = 0.3$ and for two different values of the global density. One is close to the threshold for the appearance of the B phase ($n' = 0.353$). In this case the A density is close to the density of the background and bends down close to the

interface to screen the B layer charge. Well in the bulk of A phase, where the charge density coincides with the density of the background, we have $E \sim 0$ as expected for a metal. When the global density increases the local densities decrease according to the behaviour discussed before for the average densities (figure 10). The layers become of the order of the screening length and the electric field is never completely screened.

5. Conclusions

In this work we have generalized the Maxwell construction to a situation that appears often in strongly correlated electronic systems, i.e. phase separation frustrated by the LRC interaction.

We discussed (i) the stabilization of the uniform phases as the frustrating forces are increased, (ii) the anomalous behaviour of the frustrated phase-separated state at the mesoscopic scale and (iii) the singular behaviour which results in a lattice instability when frustration dominates.

We used a UDA and a more involved LDA approach. Both approaches are shown to give very similar results, thus justifying the general use of the much simpler UDA. For the LDA we have approximated the energy functional in the case of a metal with the simplest LDA functional, i.e. the Thomas–Fermi approximation. Our formulation however is general and allows for more sophisticated functionals.

As is intuitively expected, the LRC interaction tends to stabilize the non-separated uniform phase in the presence of a rigid background. This has been illustrated in the general analysis of two generic phases described by parabolic free energies. We have shown that the region of phase separation contracts when the LRC and surface energy effects are switched on and disappears above a critical value of a dimensionless parameter λ. This parameter plays the role of an effective coupling which controls the degree of frustration and characterizes the competition between the energy cost due to the surface and Culombic energy and the energy gain in the MC. The balance between these energies determines whether the phase-separated state exists or not.

When λ is small ($\lambda < \lambda_c$) a mixed state arises. We have modelled this situation by considering a Wigner crystal of drops of one phase hosted by the other phase and a layered geometry which behaves as a one-dimensional analogue of the Wigner crystal. We believe that our general conclusions (including the existence of a critical λ) are not sensitive to the geometry of the mixed state as long as the two length scales R_c and R_d are much larger than the interparticle distance. The former length (cell size) characterizes a periodic structure and the latter (bubble size) how this periodic structure is divided to host the two phases.

In the mixed state novel nonlinear effects appear which are not present in the unfrustrated MC. Within the UDA the volume fraction and the drop radius of the minority phase do not start from zero but from a finite value and the transition to the drops state is abrupt. In the LDA physical quantities are not discontinuous but grow very steeply at the threshold mimicking the discontinuous behaviour.

An additional nonlinear effect in the drop state is that the local densities of each phase have an anomalous behaviour decreasing as the global density increases. This can affect properties of the system which are sensitive to the local density as has been shown for the Curie temperature of the manganites [7]. We emphasize that also local probes such as NMR, core spectroscopy, etc should be sensitive to this effect and may be used to detect Coulomb frustrated phase separation in real systems.

In the case of strong Coulomb interaction and large surface energy ($\lambda > \lambda_c$) a transition between two uniform phases occurs. We have shown that in this case the compressibility is singular and a lattice instability will take place if the ionic background is not fully rigid, as

in reality. The system (both electrons and ions) can separate into two neutral phases with different specific volumes.

This will also happen at the transition point between the uniform phase and the drop state although the instability is weaker. This instability can become stronger when one of the phases is incompressible. This is the case of phase separation between a metal and an insulator. λ_c diverges and the transition between the uniform metal and the drop state can happen in the presence of strong frustration. In this case the energy also has a prominent cusp which leads to a volume instability.

This scenario is in good agreement with the situation in manganites where mesoscopic phase separation appears close to a phase separation at a larger scale. The latter is characterized by the coexistence of two globally neutral phases with different unit cell volumes as found here [14, 15].

References

[1] Nagaev E 1983 *Physics of Magnetic Semiconductors* (Moscow: MIR)
[2] Castellani C, Di Castro C and Grilli M 1995 *Phys. Rev. Lett.* **75** 4650
[3] Löw U, Emery V J, Fabricius K and Kivelson S A 1994 *Phys. Rev. Lett.* **72** 1918
[4] Dagotto E, Hotta T and Moreo A 2001 *Phys. Rep.* **344** 1
[5] Hennion M *et al* 1998 *Phys. Rev. Lett.* **81** 1957
[6] Lorenzana J, Castellani C and Di Castro C 2001 *Phys. Rev.* B **64** 235127
[7] Lorenzana J, Castellani C and Di Castro C 2001 *Phys. Rev.* B **64** 235128
[8] Lorenzana J, Castellani C and Di Castro C 2002 *Europhys. Lett.* **57** 704
[9] Lawrence J M, Riseborough P S and Parks R D 1981 *Rep. Prog. Phys.* **44** 1
[10] Wigner E 1934 *Phys. Rev.* **46** 1002
[11] Mahan G D 1990 *Many Particle Physics* (New York: Plenum)
[12] Nagaev E, Podel'shchikov A I and Zil'bewarg V E 1998 *J. Phys.: Condens. Matter* **10** 9823
[13] Bustingorry S, Jagla E and Lorenzana J 2003 *Phys. Rev. Lett.* (submitted)
[14] Uehara M, Mori S, Chen C and Cheong S-W 1999 *Nature* **399** 560
[15] Cox D E, Radaelli P G, Marezio M and Cheong S W 1998 *Phys. Rev.* B **57** 3305